Hydrogels

International Edition: DOI: 10.1002/anie.201411875
German Edition: DOI: 10.1002/ange.201411875

Fibrillar Networks of Glycyrrhizic Acid for Hybrid Nanomaterials with Catalytic Features**

*Abhijit Saha, Jozef Adamcik, Sreenath Bolisetty, Stephan Handschin, and Raffaele Mezzenga**

Abstract: *Self-assembly of the naturally occurring sweetening agent, glycyrrhizic acid (GA) in water is studied by small-angle X-ray scattering and microscopic techniques. Statistical analysis on atomic force microscopy images reveals the formation of ultralong GA fibrils with uniform thickness of 2.5 nm and right-handed twist with a pitch of 9 nm, independently of GA concentration. Transparent nematic GA hydrogels are exploited to create functional hybrid materials. Two-fold and three-fold hybrids are developed by introducing graphene oxide (GO) and in situ-synthesized gold nanoparticles (Au NPs) in the hydrogel matrix for catalysis applications. In the presence of GO, the catalytic efficiency of Au NPs in the reduction of p-nitrophenol to p-aminophenol is enhanced by 2.5 times. Gold microplate single crystals are further synthesized in the GA hydrogel, expanding the scope of these hybrids and demonstrating their versatility in materials design.*

Exploiting self-assembly of small molecules,[1–4] especially naturally occurring molecules or their derivatives[5] as building blocks for functional materials, is beneficial in terms of bioavailability, biocompatibility, and biodegradability. The anisotropic assembly of small molecules leads to the formation of one-dimensional (1D) nanostructures such as fibrils, ribbons, tapes, and nanotubes in water, which, upon increasing concentrations can further form network structures, and—provided the network is strong enough—also form hydrogels.[6] A hydrogel is a versatile matrix for the encapsulation of various drugs as well as inorganic, organic, and carbon nanostructures, to form functional hybrid systems.[7] Among all the carbon materials, graphene and GO nanosheets have become a very exciting subject of research in the last few years because of their large specific surface area, high conductivity, and extraordinary mechanical strength.[8,9] Graphene/GO-based functional nanohybrids/composites have been developed recently in combination with other nanoscale building blocks such as fibrils and NPs, with particular focus on catalysis and sensing.[10] Yet, three-fold hybrids comprising graphene/GO, nanofibrils, and metallic NPs remain scarce[11] despite the possible wider functionalities. This paper reports the design of a three-fold nanosystem composed of GO, metallic NPs, and self-assembled nanofibrils of GA for tunable catalysis.

GA is a natural saponin, a major ingredient of licorice and is widely used in candies and sweets. It has 50 times the sweetening power of sucrose and is also used as drug for the treatment of liver cell injury, chronic viral hepatitis, and skin diseases.[12] GA has a hydrophobic triterpenoid aglycon moiety (18β-glycyrrhetinic acid) attached to a hydrophilic diglucuronic unit. Owing to both of its hydrophobic and hydrophilic moieties, it has an amphiphilic nature and an expected complex self-assembly behavior in water. Self-assembly of GA is investigated as a function of concentration, and on increase of it, an isotropic fluid, a nematic phase and a hydrogel are found, progressively. The hydrogel of GA nanofibrils is further combined with other building blocks (GO and Au NPs) to design functional hybrid nanomaterials. In the presence of GO, the catalytic efficiency of Au NPs is found to be improved in the reduction of *p*-nitrophenol (PNP) to *p*-aminophenol (PAP).[13] The shape of Au NPs, which enable catalysis, can be adjusted from spherical nanoparticles to microplate single crystals.[14] Thus the hybrids possess tunable catalytic function and structural features.

Samples of various concentrations of GA were scanned by atomic force microscopy (AFM; Figure S1a–d) to understand the mechanism of self-assembly. The sample with 0.025 wt% of GA showed a few very thin fibrils (Figure S1a). Gradual increase in concentration of GA molecules resulted in a denser coverage of the mica substrate by the self-assembled fibrils. A larger population of fibrils with a length of tens of micrometers was found at a concentration of 0.05 wt% in equilibrium with a lower amount of monomers in solution (Figure S1b). Interestingly, at a concentration of 0.1 wt%, almost all of the monomers aggregated to form fibrils with minimum detectable monomers remaining in equilibrium in solution (Figure S1c) and at a concentration of 0.25 wt% the GA fibrils covered the whole surface of the mica substrate (Figure S1d). Figure 1a displays three-dimensional (3D) AFM images with an enlarged part of 0.1 wt% GA fibrils (Figure 1b) showing right-handedness of fibrils (Figure 1c) with a height of 2.5 nm and periodicity of 9 nm according to longitudinal and transversal height profiles, respectively (Figure 1d). The sample with 0.25 wt% of GA was highly viscous. With gradual increase of the concentration of GA, it formed a transparent gel at the very low concentration of 0.3 wt% (Figure S2a). A frequency sweep measurement of 2 wt% hydrogel of GA (Figure S2a and b) revealed the formation of a viscoelastic network of GA (Figure S2c). The AFM images of a thin layer of 2 wt% hydrogel (Figures 1h–j

[*] Dr. A. Saha, Dr. J. Adamcik, Dr. S. Bolisetty, Prof. Dr. R. Mezzenga
Laboratory of Food & Soft Materials Science
Institute of Food, Nutrition & Health
Department of Health Sciences & Technology, ETH Zürich
Schmelzbergstrasse 9, LFO E23, 8092 Zürich (Switzerland)
E-mail: raffaele.mezzenga@hest.ethz.ch

[**] We acknowledge supports of ScopeM/ETH Zürich, for TEM and Lothar Opilik, ETH Zürich, for Raman measurements. The authors acknowledge the Swiss National Science Foundation (SNSF, project no. 200021_135146) for financial support.

Supporting information for this article is available on the WWW under http://dx.doi.org/10.1002/anie.201411875.

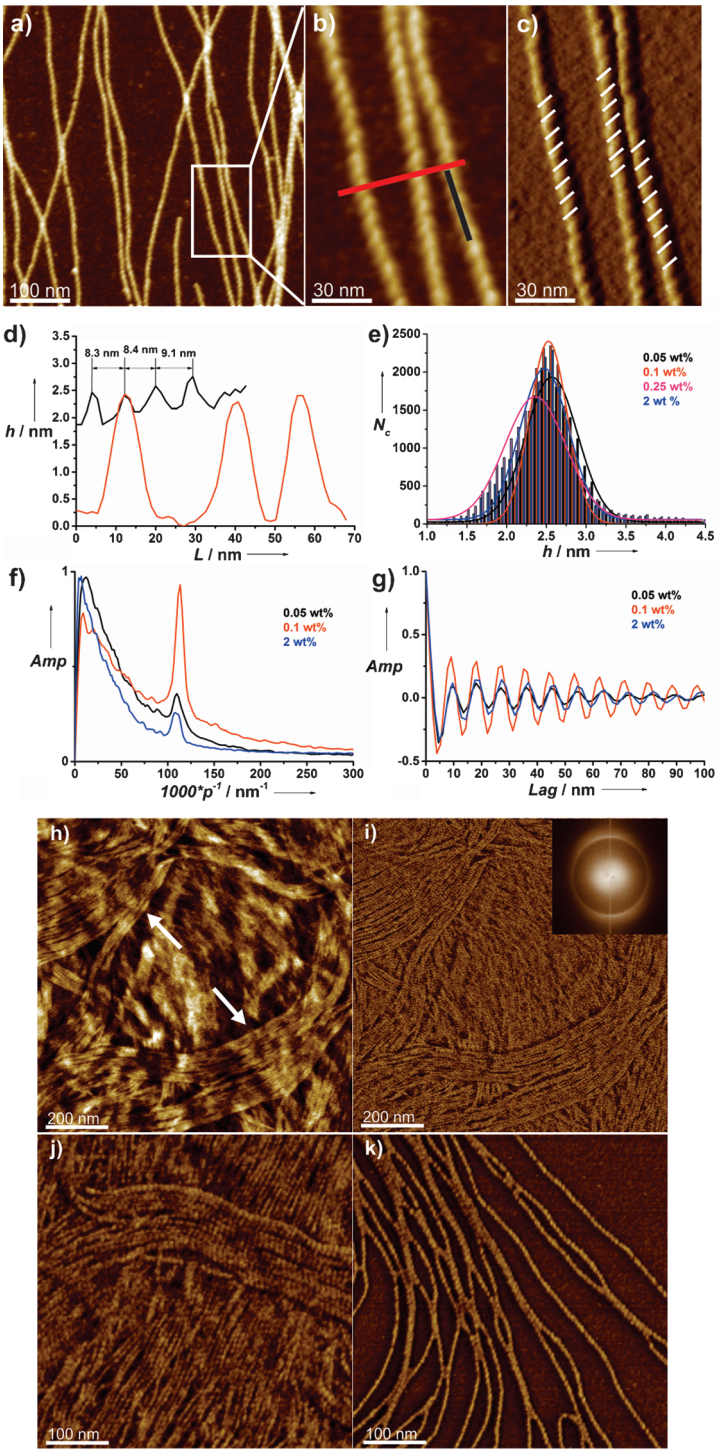

Figure 1. a) 3D AFM image of 0.1 wt% sample of GA fibrils; b) magnified image of selected area in panel (a); c) AFM amplitude image of panel (b) with labeled direction of the chirality of GA fibrils; d) the longitudinal (black curve) and transversal (red curve) height profile of GA fibrils from panel (b); e) the maximum height histogram of GA fibrils assembled in water at different concentrations; the pitch size estimation by f) FFT analysis of the height profiles, g) averaged autocorrelation functions of the twisted-angle profiles along the fibril middle lines for 0.05 wt%, 0.1 wt%, and 2 wt% GA fibrils; h) AFM height image of a thin layer of the 2 wt% GA hydrogel and i) corresponding AFM phase image with the inset representing the FFT analysis of AFM phase image. j) AFM phase image of the layer of 2 wt% GA hydrogel and k) AFM phase image of individual GA fibrils of the 2 wt% GA hydrogel.

and S1e and f) showed the formation of thin layers of highly aligned fibrils with random spatial orientation in the hydrogel (see the arrows in Figure 1h) whereas the AFM phase image (Figure 1i) showed that fibrils possess an internal structure with a periodicity around 9 nm according to fast Fourier transform analysis (FFT) of image (inset in Figure 1i). The individual GA fibrils observed at the edge of the hydrogel (Figures 1k and S1g–l) have morphology (right-handedness) similar to the fibrils assembled at lower GA concentrations, suggesting the formation of uniform fibrils independently of the concentration of GA. For detailed analysis of the morphology of GA fibrils assembled at different concentrations, parameters of GA fibrils obtained at various concentrations of GA in water, such as average height and pitch size of the periodicity, were evaluated from a systematic statistical analysis performed on the extracted coordinates.

These processing and tracking routines have recently been applied to perform statistical analysis of amyloid fibrils,[15a,b] supramolecular fibrils,[15c] and also charged linear polysaccharides.[15d] An advantage of using this procedure is a large number of accessible coordinates for significant statistical analysis. Figure 1e represents the height distribution of 0.05 wt%, 0.1 wt%, 0.25 wt%, and 2 wt% GA fibrils showing that the fibrils possess uniform height of 2.5 nm. Figure 1f and g display the results for the pitch size estimation of 0.05 wt%, 0.1 wt%, and 2 wt% of GA fibrils by FFT analysis of the height profiles and averaged autocorrelation functions of the twisted-angle profiles along the fibril middle lines, respectively. In both cases the pitch size is 9 nm for all GA concentrations.

Thin layers of 2 wt% GA hydrogel exhibited a strong birefringence under the polarized optical microscope (POM; Figure 2a). This is indicative of anisotropic aggregation of the GA monomers into an ordered nematic mesophase (Figure S2b) as also evidenced from AFM imaging. To investigate the structure of the nematic mesophase of the 2 wt% hydrogel, the sample was further studied by SAXS measurements. The two-dimensional scattering profile (Figure 2b) shows an anisotropic scattering intensity pattern in the low scattering vector region ($q \leq 0.027$ Å^{-1}) which confirms the alignment of structures in the solution. The radially averaged SAXS scattering intensity (Figure 2c) in the q region between 0.027 Å^{-1} and 0.08 Å^{-1} follows a slope of −1.64. This scattering slope further confirms the form factor of semiflexible fibrils in analogy with the expected 5/3 fractal exponent for self-avoiding random walks in a good solvent. In the high q region, the scattering pattern follows the Porod decay (slope −4) due to the sharp interface of the fibril surfaces. To quantify the order of the fibrils, the scattering pattern was azimuthally plotted in Figure 2d. The two polar maxima in the azimuthal pattern indicate the horizontal alignment of the fibrils.

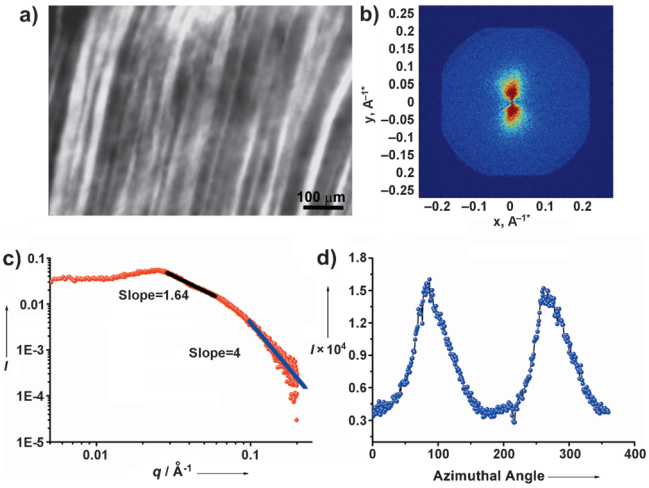

Figure 2. a) POM image, b) 2D SAXS diffractogram, c) radial intensity evolution of the scattered intensity, and d) azimuthal SAXS intensity from the 2 wt% GA hydrogel.

This indicates that the excluded volume among fibrils is directed by the geometry of the capillary, inferring a very long-range order (of the length scale of the SAXS beam, that is, 700 μm). The 3D order parameter was calculated by using Equation (3) (Supporting Information, SI) in the q region of 0.005 $Å^{-1}$ to 0.027 $Å^{-1}$, yielding a value of 0.37, in further support of a high degree of spatial alignment of the fibrils.

To further elucidate the fibrillar structure of GA in water, wide-angle X-ray scatterings (WAXS) was performed on the lyophilized 2 wt% hydrogel of GA (Figure S3). Peaks at 0.223, 0.55, 1.029, and 1.43 $Å^{-1}$ were observed corresponding to 28.2, 11.4, 6.1, and 4.4 Å, respectively. 2.8 nm is larger than the energy minimized molecular length of GA (18.6 Å) but less than 2x the GA length, thereby suggesting that the hydrophobic triterpenoid moieties of GA molecules can interact laterally, tilting in a head-to-head way and leaving the hydrophilic diglucuronic groups exposed to water (Scheme 1). The diameter of fibril obtained from WAXS study (2.8 nm) is also in good agreement with the height profile of fibrils from AFM measurements (2.5 nm). The length of 11.4 Å may correspond to the length of the hydrophilic diglucuronic part of GA, whereas the shortest length scale of 4.4 Å captures the close packing of the moieties along the fibrils. The right-handed twist arises from an amplified supramolecular chirality of the chiral triterpenoid moieties of GA.

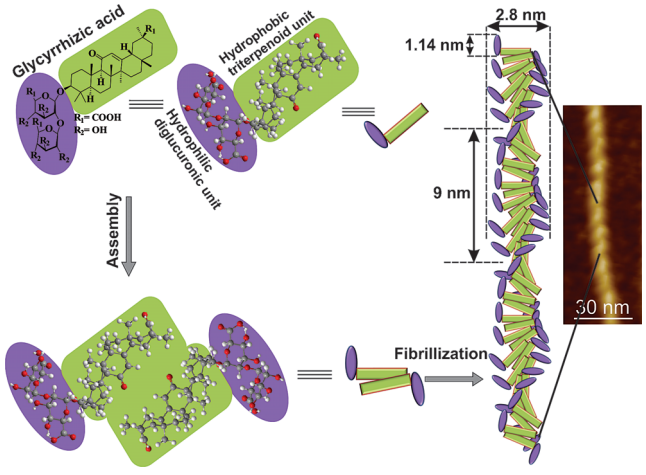

Scheme 1. Sketch of fibril formation by self-assembly of GA in water.

We then explored the possibility of creating hybrid systems from the GA hydrogels. The amphiphilic nature of GA allows for further functionalization. We considered GO, capable of π–π and hydrophobic interactions,[16a] as a suitable component to functionalize the hydrogel matrix. The hydrophobic triterpenoid is likely to interact in water with the hydrophobic aromatic surface of GO yielding a deep-brown colored two-fold GA–GO hybrid hydrogel (Figure S4). The diglucuronic moiety of GA can reduce the chloroauric acid to Au NPs in the hydrogel and hence the use of any external reducing agent (e.g., $NaBH_4$) is not required. The development of reddish hydrogels (Figure S4) with a surface plasmon resonance absorption peak at 524 nm (Figure S5) is indicative of the in situ reduction of gold salt by the diglucuronic moiety of GA to metallic Au NPs.[14a] Finally, a complex black-colored three-fold system was produced in the GA hydrogel by simultaneously incorporating both GO and chloroauric acid into the solution of GA (Figure S4). The hybrid systems were scanned by AFM to reveal the morphology (Figure S6a–i). AFM (Figure S6g–i) and TEM (Figure S7) images of the three-fold hydrogel hybrid show coexistence of GA nanofibrils, GO nanosheets, and Au NPs in the hydrogel matrix. In the GA–Au NP hybrid the diameter of Au NPs varies from 2 to 35 nm (Figure S8a and c). Similarly, in the three-fold hybrid system, the diameter of Au NPs ranges from 2 to 26 nm (Figure S8b and d). High-resolution TEM of the GA–Au NP hybrid revealed nanocrystalline particles with atomic planes spacing clearly visible (Figure S9a and b). Furthermore, energy-dispersive X-ray analysis (EDX) also confirmed the composition of Au (Figure S9c). Raman spectroscopic analysis (Figure S10) for the two GO-containing hybrids (GA–GO and GA–GO–Au NP) indicates that GA molecules in both the hybrid hydrogels do not reduce the GO[10d,16b] but do reduce gold salt (Au^{3+}) to Au NPs at room temperature.

Au NPs can act as catalyst in various electron-transfer processes such as in the heterogeneous catalytic reduction of PNP to PAP (Figure 3a, inset) in the presence of reducing agents such as $NaBH_4$.[11b,13] Here PNP was chosen as a model substrate for the reduction reaction in aqueous medium, and to assess the influence of GO in the catalytic activity of Au NPs in the three-fold hybrid. In alkaline medium, due to the formation of the p-nitrophenolate ion, PNP shows a strong absorption peak at 400 nm which disappears with time and a new peak at ca. 300 nm appears (Figure 3a,b) as conversion of PNP to PAP proceeds. The kinetics of the reduction is followed by plotting the absorption at 400 nm (A) versus time (Figure 3c). For the two-fold catalyst, it takes 10 min to complete the reaction (Figure 3c, red line). Interestingly, at the same concentrations, the PNP is reduced within 6 min by the three-fold catalyst (Figure 3c, black line). Control experiments were run to demonstrate that there is no reduction of PNP in the absence of Au NPs under similar conditions (with either GA or GA–GO hydrogels). The rate of catalysis (K_{cat})

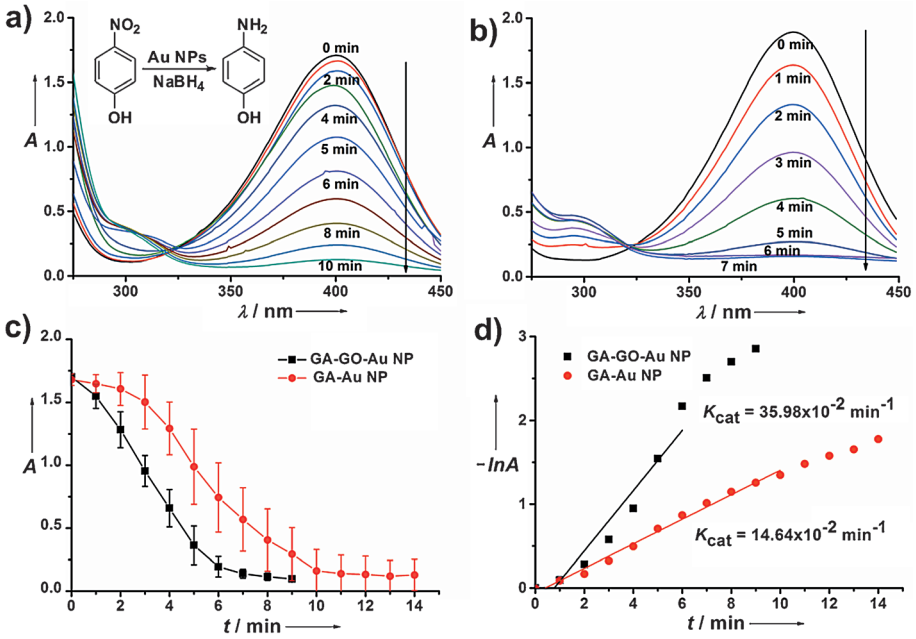

Figure 3. UV-Visible spectra of the catalytic reduction of PNP to PAP by: a) GA–Au NP catalyst (Inset: Scheme for the reduction of PNP to PAP by Au NPs), b) by GA–GO–Au NP catalyst, c) plot of absorption at 400 nm (A) versus t (min) and d) plot of $-\ln A$ versus t (min) for the catalytic reduction of PNP to PAP in the two systems.

can be determined from the slope of the plot of $-\ln A$ ($A = A_{400\,nm}$) versus time (SI). The K_{cat} by the two-fold system is calculated to be 14.6×10^{-2} min^{-1}; the same for the three-fold catalyst is 36.0×10^{-2} min^{-1} (Figure 3d). With 2.5 times faster reaction rate, the three-fold catalyst is more efficient than the two-fold catalyst[12b] although both hybrids contain an identical amount of Au NPs. It is also to be noted that the plot of $-\ln A$ versus time is linear for the two-fold catalyst but in the case of the three-fold catalyst, the plot deviates into a sigmoidal profile, suggesting a slightly different catalysis mechanism in the presence of GO. Because of the π–π interactions between the large surface of GO and PNP, the effective concentration of PNP is increased in the vicinity of Au NPs immobilized on the GO surface, which may have a synergistic effect on the catalytic reaction. To verify this, we performed a very conservative control experiment. We monitored the reduction of PNP to PAP in GA–GO hydrogels mixed with commercially synthesized Au NPs having a diameter (5 nm) well below the average diameter of the two- and three-fold hybrids, keeping the weight concentration of gold equal to that of the Au-containing two- and three-fold hybrids. Yet, we observed that neither the reduction was as fast as in the case of the three-fold system nor did it follow the same kinetic pathway (Figure S11). This observation clearly indicates that immobilization of reduced Au NPs onto the GO surface is central for the improved catalytic activity of the corresponding hybrid system, offering the appealing property to modulate catalytic properties.

We finally show also the size and shape of Au NPs in the GA hydrogel matrix can be efficiently tuned by increasing the concentration (10x) to 4.1 mM of the precursor, chloroauric acid, while maintaining the concentration of GA constant (2 wt %). AFM and TEM imaging on the sample showed formation of giant plate-like structures of micrometers lateral size with hexagonal, triangular, and polygonal shapes (Figures S12 and S13).[14] Careful observation of AFM images reveals that the plates are densely coated by GA fibrils. The first step in the reduction of precursor salt to NPs by the fibrils diglucuronic groups occurs through the nucleation and growth of the Au NPs.[14a] As the size of the growing Au NPs becomes larger than the dimension of the GA fibrils, more fibrils are required to cooperatively assist the growth of the Au NPs. It is the nematic liquid crystalline hydrogel matrix, which directs the subsequent growing and formation of giant Au microplates. Thus the nematic mesophase of self-assembled fibrils of GA plays a major role in directing the morphology of NPs.

In summary we have shown that the naturally occurring chiral saponin GA self-assembles in water into long fibrils with right-handed twist, 9 nm periodicity, and 2.5 nm thickness, independently of GA concentration. Increase in the concentration of GA resulted in the formation of nematic phases first and hydrogels afterwards. These nanofibrils were further investigated as scaffolds for functional hybrids of use in heterogeneous catalysis. The hydrophobic triterpenoid groups of GA fibrils interact with the aromatic surface of GO, while the diglucuronic moiety allows reduction of gold salt (Au^{3+}) to Au NPs and microcrystals. A complex three-fold catalyst system was developed inclusive of GA nanofibrils, Au NPs, and GO. Due to the interactions between the GO and the catalysis substrate, a synergistic effect of GO and Au NPs was observed leading to an improved catalytic efficiency. These results may open new scenarios on the design of advanced hybrid materials for catalysis using natural precursors and affordable building blocks.

Keywords: glycyrrhizic acid · nanohydbrid hydrogels · self-assembly · statistical analysis · tuneable catalysis

How to cite: *Angew. Chem. Int. Ed.* **2015**, *54*, 5408–5412
Angew. Chem. **2015**, *127*, 5498–5502

[1] T. Aida, E. W. Meijer, S. I. Stupp, *Science* **2012**, *335*, 813–817.
[2] T. F. A. De Greef, M. M. J. Smulders, M. Wolffs, A. P. H. J. Schenning, R. P. Sijbesma, E. W. Meijer, *Chem. Rev.* **2009**, *109*, 5687–5754.
[3] S. I. Stupp, L. C. Palmer, *Chem. Mater.* **2014**, *26*, 507–518.
[4] a) E. Busseron, Y. Ruff, E. Moulin, N. Giuseppone, *Nanoscale* **2013**, *5*, 7098–7140; b) A. Zielinska, M. Leonowicz, H. Li, T. Nakanishi, *Curr. Opin. Colloid Interface Sci.* **2014**, *19*, 131–139;

c) S. S. Babu, V. K. Praveen, A. Ajayaghosh, *Chem. Rev.* **2014**, *114*, 1973 – 2129.
[5] a) A. Saha, S. Manna, A. K. Nandi, *Langmuir* **2007**, *23*, 13126 – 13135; b) L. Schefer, A. Sánchez-Ferrer, J. Adamcik, R. Mezzenga, *Langmuir* **2012**, *28*, 5999 – 6005; c) Nonappa, U. Maitra, *Org. Biomol. Chem.* **2008**, *6*, 657 – 669; d) J. H. Jung, S. Shinkai, T. Shimizu, *Chem. Eur. J.* **2002**, *8*, 2684 – 2690; e) A. Sánchez-Ferrer, J. Adamcik, R. Mezzenga, *Soft Matter* **2012**, *8*, 149 – 155; f) A. Saha, B. Roy, A. Garai, A. K. Nandi, *Langmuir* **2009**, *25*, 8457 – 8461; g) A. Saha, S. Bolisetty, S. Handschin, R. Mezzenga, *Soft Matter* **2013**, *9*, 10239 – 10242.
[6] L. A. Estroff, A. D. Hamilton, *Chem. Rev.* **2004**, *104*, 1201 – 1218.
[7] a) M. de Loos, B. L. Feringa, J. H. van Esch, *Eur. J. Org. Chem.* **2005**, 3615 – 3631; b) F. Zhao, M. L. Ma, B. Xu, *Chem. Soc. Rev.* **2009**, *38*, 883 – 891; c) A. Döring, W. Birnbaum, D. Kuckling, *Chem. Soc. Rev.* **2013**, *42*, 7391 – 7420; d) D. Das, T. Kar, P. K. Das, *Soft Matter* **2012**, *8*, 2348 – 2365.
[8] A. K. Geim, K. S. Novoselov, *Nat. Mater.* **2007**, *6*, 183 – 191.
[9] a) D. Li, R. B. Kaner, *Science* **2008**, *320*, 1170 – 1171; b) C. N. R. Rao, A. K. Sood, K. S. Subrahmanyam, A. Govindaraj, *Angew. Chem. Int. Ed.* **2009**, *48*, 7752 – 7777; *Angew. Chem.* **2009**, *121*, 7890 – 7916.
[10] a) S. Navalon, A. Dhakshinamoorthy, M. Alvaro, H. Garcia, *Chem. Rev.* **2014**, *114*, 6179 – 6212; b) C. Li, J. Adamcik, R. Mezzenga, *Nat. Nanotechnol.* **2012**, *7*, 421 – 427; c) M. Stürzel, Y. Thomann, M. Enders, R. Mülhaupt, *Macromolecules* **2014**, *47*, 4979 – 4986; d) S. Yang, J. Dong, Z. Yao, C. Shen, X. Shi, Y. Tian, S. Lin, X. Zhang, *Sci. Rep.* **2014**, DOI: 10.1038/srep04501.
[11] a) J. Wang, X. Zhao, J. Li, X. Kuang, Y. Fan, G. Wei, Z. Su, *ACS Macro Lett.* **2014**, *3*, 529 – 533; b) J. Nanda, A. Biswas, B. Adhikari, A. Banerjee, *Angew. Chem. Int. Ed.* **2013**, *52*, 5041 – 5045; *Angew. Chem.* **2013**, *125*, 5145 – 5149.
[12] a) M. N. Asl, H. Hosseinzadeh, *Phytother. Res.* **2008**, *22*, 709 – 724; b) L. A. Baltina, R. M. Kondratenko, L. A. Baltina, O. A. Plyasunova, A. G. Pokrovskii, G. A. Tolstikov, *Pharm. Chem. J.* **2009**, *43*, 539 – 548.
[13] a) K. Hayakawa, T. Yoshimura, K. Esumi, *Langmuir* **2003**, *19*, 5517 – 5521; b) S. Wunder, F. Polzer, Y. Lu, Y. Mei, M. Ballauff, *J. Phys. Chem. C* **2010**, *114*, 8814 – 8820.
[14] a) S. Bolisetty, J. J. Vallooran, J. Adamcik, S. Handschin, F. Gramm, R. Mezzenga, *J. Colloid Interface Sci.* **2011**, *361*, 90 – 96; b) B. J. Wiley, D. J. Lipomi, J. Bao, F. Capasso, G. M. Whitesides, *Nano Lett.* **2008**, *8*, 3023 – 3028; c) C. Li, S. Bolisetty, R. Mezzenga, *Adv. Mater.* **2013**, *25*, 3694 – 3700.
[15] a) I. Usov, J. Adamcik, R. Mezzenga, *ACS Nano* **2013**, *7*, 10465 – 10474; b) J. Adamcik, J.-M. Jung, J. Flakowski, P. De Los Rios, G. Dietler, R. Mezzenga, *Nat. Nanotechnol.* **2010**, *5*, 423 – 428; c) L. Albertazzi, D. van der Zwaag, C. M. A. Leenders, R. Fitzner, R. W. van der Hofstad, E. W. Meijer, *Science* **2014**, *344*, 491 – 495; d) L. Schefer, J. Adamcik, R. Mezzenga, *Angew. Chem. Int. Ed.* **2014**, *53*, 5376 – 5379; *Angew. Chem.* **2014**, *126*, 5480 – 5483.
[16] a) F. Kim, L. J. Cote, J. Huang, *Adv. Mater.* **2010**, *22*, 1954 – 1958; b) K. N. Kudin, B. Ozbas, H. C. Schniepp, R. K. Prud'homme, I. A. Aksay, R. Car, *Nano Lett.* **2008**, *8*, 36 – 41.

Received: December 14, 2014
Revised: February 13, 2015
Published online: March 10, 2015

